Mixed-Domain Adaptive Blind Correction of High-Resolution Time-Interleaved ADCs

Munkyo Seo, Eunsoo Nam, and Mark Rodwell

Blind mismatch correction of time-interleaved analog-to-digital converters (TI-ADC) is a challenging task. We present a practical blind calibration technique for low-computation, low-complexity, and high-resolution applications. Its key features are: dramatically reduced computation; simple hardware; guaranteed parameter convergence with an arbitrary number of TI-ADC channels and most real-life input signals, with no bandwidth limitation; multiple Nyquist zone operation; and mixed-domain error correction. The proposed technique is experimentally verified by an $M = 4$ 400 MSPS TI-ADC system. In a single-tone test, the proposed practical blind calibration technique suppressed mismatch spurs by 70 dB to 90 dB below the signal tone across the first two Nyquist zones (10 MHz to 390 MHz). A wideband signal test also confirms the proposed technique.

Keywords: Analog-to-digital conversion, mismatch, blind algorithm, adaptive technique.

I. Introduction

A time-interleaved analog-to-digital converter (TI-ADC) is a scalable architecture for very high sampling rates. A number of subconverters cyclically sample the input signal, and multiple outputs are combined to yield a single digital stream (Fig. 1 (a)). The collective sampling rate is, therefore, proportional to the number of subconverters. It has been well known, however, that the spectral performance of a TI-ADC is limited by aliasing spectra due to mismatches in subconverter gain, sampling time, and so on [1]–[6].

Currently known mismatch correction techniques can be categorized into training (foreground) [2], [6] and blind (background) methods [7]–[26]. Training methods are suitable for high-resolution application in general, since they are capable of correcting general linear mismatches [6], but at the cost of suspension of data acquisition during each calibration. They are also subject to post-calibration detuning due to temperature variation, aging, and so on [6]. Blind methods, on the other hand, use normal input signals for calibration purposes; therefore, they do not require a dedicated calibration period. Errors that slowly vary as a function of time may also be tracked. There have been proposed a variety of blind methods with different accomplishments and limitations. One group of techniques performs error detection and error correction entirely in the digital domain [7]–[17], as illustrated in Fig. 1(b). Another class of techniques use both the analog and digital domain [18]–[26].

Previous mixed-domain methods typically involve special analog signal processing (for example, adding a known signal to the input, as in Fig. 1 (c)), to facilitate mismatch estimation, which may potentially compromise input signal integrity. Purely digital techniques keep the analog signal path intact, but

Manuscript received Jan. 24, 2014; revised July 3, 2014; accepted July 18, 2014.

This work was supported by the National Research Foundation of Korea (NRF) grant funded by the Korea Government (MEST) (No. 2013-056424).

Munkyo Seo (corresponding author, mkseo@ieee.org) is with the College of Information and Communication Engineering, Sungkyunkwan University, Suwon, Rep. of Korea.

Eunsoo Nam (esnam@etri.re.kr) is with the Components & Materials Research Laboratory, ETRI, Daejeon, Rep. of Korea.

Mark Rodwell (rodwell@ece.ucsb.edu) is with the Department of Electrical and Computer Engineering, University of California, Santa Barbara, USA.

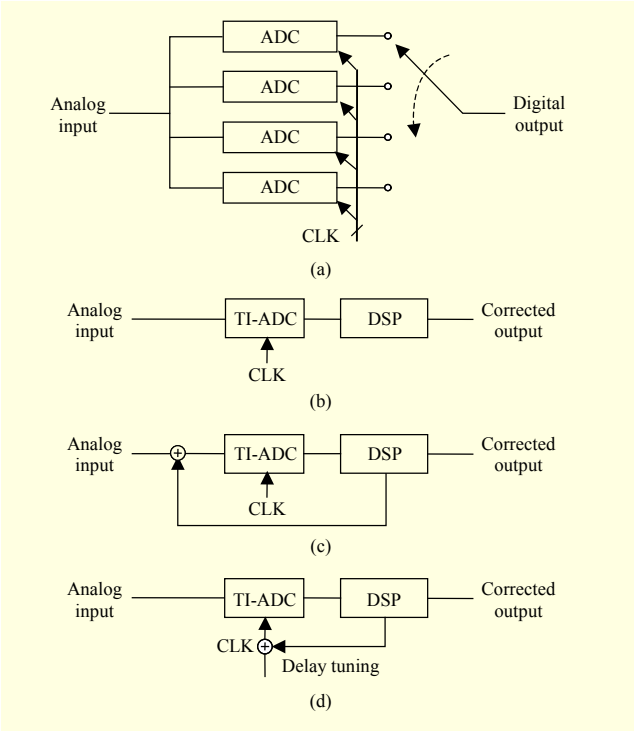

Fig. 1. (a) TI-ADC system, (b) TI-ADC with full digital-domain blind correction, (c) conventional mixed-domain method with analog input pre-processing, and (d) proposed mixed-domain method with sampling clock tuning.

their computational cost is highly demanding. This is partly due to the complex parameter search algorithm, but mostly due to digital correction of sampling time delay, since matrix inversion or transformation between the time and frequency domains is usually required for correction filter calculation. Further, the resulting correction filter is long (sinc(t) decays only as $1/t$), increasing hardware cost and complexity. Depending on blind correction algorithms, the estimation of timing error may also be computationally complex. For both classes of techniques, special assumptions are necessary (for example, reduced input bandwidth, limited number of TI-ADC channels, or wide-sense stationarity) to make the problem of blind estimation solvable. Full-digital techniques tend to require stronger assumptions; thus, they are more restrictive than mixed-domain methods. Using an extra ADC may provide a convenient calibration reference, but the analog input path is subject to switching, which raises concerns about signal integrity.

The above discussion naturally leaves us one interesting option in the mixed-domain: timing error correction in the analog domain by directly tuning sampling clocks (Fig. 1 (d)). This obviates long digital filters as well as their online calculation for timing correction. In addition, timing correction can now be perfect over *multiple* Nyquist zones. In contrast, a single set of digital filters can only provide approximate timing correction over a single Nyquist zone, due to limited usable bandwidth and in-band ripples, among others. We must still develop a reliable blind estimation method to close the feedback loop, preferably with weaker working assumptions so as to allow application to the widest range of signals.

In accordance with the above discussion, the authors previously reported a new mixed-domain blind method with analog tuning of sampling clocks [26]. This paper presents a full-fledged discussion with theory and new experimental results. Dramatically reduced computational complexity and exceptionally wide applicability are among the contributions of the paper. The proposed blind method is based on the assumption that the input signal is wide-sense stationary (WSS). Under the input WSS assumption, the mismatch estimates are guaranteed to converge to true parameters. No further restriction on the input signal is necessary. Specifically, the TI-ADC can have an arbitrary number of channels, with no need of an additional subconverter for calibration reference. The input spectrum can cover the full Nyquist bandwidth. In fact, the proposed blind method works in any Nyquist zone.

Similar mixed-domain approaches have been proposed [23]–[25], with their own assumptions and restrictions: it is unclear whether the correction method in [23] applies to wideband signals. The proposed method in [24] only applies to random data; for example, digitally modulated signals. An additional subconverter channel is necessary in [25] for calibration reference.

Section II describes our system model. Section III introduces the proposed error detection method, and Section IV develops the proposed error detection method's adaptive implementation for parameter estimation. Section V discusses the experimental results, and Section VI concludes the paper.

II. System Model

Figure 2 shows a block diagram of the $M = 4$ TI-ADC with the proposed mismatch correction scheme. Each of the four subconverters successively samples the input signal, $x(t)$, every $4T_s$ such that the overall sampling rate is f_s (= $1/T_s$). Listed below are pertinent assumptions and clarifications relating to the proposed mismatch correction scheme.

- The input $x(t)$ is WSS and bandlimited from dc to $f_s/2$. No further information about $x(t)$ is known.
- The mismatch in subconverter dc offsets is independently corrected by first measuring and then subsequent subtracting.
- The kth channel subconverter has *intrinsic* gain G^*_k and sampling time error Δt^*_k, both of which are unknown.
- The *estimate* of the intrinsic gain and sampling time errors is $\tilde{G}_k$ and $\Delta\tilde{t}_k$, respectively.

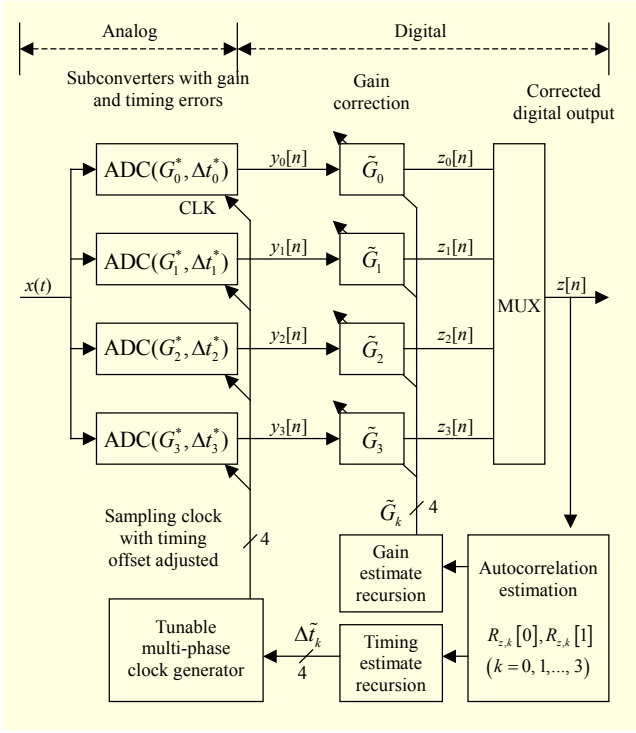

Fig. 2. $M = 4$ TI-ADC system with proposed mismatch correction scheme.

- Correction of sampling time mismatches is achieved by tuning individual sampling clocks to the estimate $\Delta\tilde{t}_k$.
- Correction of gain error is performed by digitally dividing the subconverter output by the gain estimate $\tilde{G}_k$.
- *Residual* mismatch error is defined as the difference between intrinsic and estimated parameters.
- The magnitude of intrinsic mismatches is small. The precise interpretation will be made clear in the context.

The output of the kth subconverter, $y_k[n]$, is

$$y_k[n] = G_k^* x\left((Mn+k)T_s + \Delta t_k^* - \Delta\tilde{t}_k\right),$$

where M is the number of TI-ADC channels. After gain correction, we have

$$z_k[n] = \frac{y_k[n]}{\tilde{G}_k}. \tag{1}$$

Therefore, the subsequence $z_k[n]$ is a scaled, time-shifted, and undersampled version of $x(t)$ and is given as

$$z_k[n] = \left[\frac{G_k^*}{\tilde{G}_k}\right]\left[x\left((Mn+k)T_s + \Delta t_k^* - \Delta\tilde{t}_k\right)\right] \text{ for } k = 0, \ldots, M-1. \tag{2}$$

The overall TI-ADC output, $z[n]$, is obtained by taking $z_k[n]$'s in a cyclic fashion as follows:

$$z[n] = z_{n \bmod M}\left[\text{floor}\left(\frac{n}{M}\right)\right], \tag{3}$$

where floor(x) is the greatest integer less than or equal to x.

1. TI-ADC Mismatch Model

If there is no residual mismatch, then it follows from (2)–(3) that $z[n] = x(nT_s)$ — a perfect reconstruction of the input. Otherwise, $z[n]$ is modulated by residual gain or sampling time errors. In the frequency domain, this modulation manifests itself as frequency-shifted input spectra, known as aliasing error. Aliasing effects of gain and sampling time error have been extensively studied [1], [3]–[5]. In this section, we briefly review the generalized mismatch model [6]. Let $H_k(f)$ be the frequency response of the kth channel (which includes static gain and time delay as a special case). The spectrum of $z[n]$ consists of linearly weighted frequency-shifted input spectra [6] and is as follows:

$$Z\left(e^{j2\pi f}\right) = \sum_{m=0}^{M-1} c_m\left(f - \frac{m}{M}f_s\right) X\left(f - \frac{m}{M}f_s\right), \tag{4}$$

where $Z(e^{j2\pi f})$ and $X(f)$ are the Fourier transform of $z[n]$ and $x(t)$, respectively. The conversion gains, $c_m(f)$'s, are obtained by taking the discrete Fourier transform (DFT) of the $H_k(f)$'s with respect to k. If there is no mismatch, then the $H_k(f)$'s are all equal. The only nonzero DFT coefficient in this case is $c_0(f)$ — the average of the $H_k(f)$'s.

2. Adjacent-Channel Timing Offset

It will prove to be useful to use the *adjacent-channel timing offset*, δ_k, between two cyclically neighboring channels; thus, we have

$$\delta_k \equiv \Delta t_{k+1} - \Delta t_k \qquad \text{for } k = 0, \ldots, M-2. \tag{5}$$

The δ_k's do not retain the common timing offset in sampling instances, but the timing *mismatch* information is still preserved. To retrieve the Δt_k's from the δ_k's (to drive the tunable sampling clock), we need an additional constraint. Two reasonable choices are as follows:

$$\Delta t_k = \sum_{n=0}^{k-1}\delta_n \quad \text{assuming } \Delta t_0 = 0 \tag{6}$$

or

$$\Delta t_k = \sum_{n=0}^{k-1}\delta_n - \frac{1}{M}\sum_{m=0}^{M-2}(M-1-m)\delta_m \quad \text{assuming } \sum_{k=0}^{M-1}\Delta t_k = 0. \tag{7}$$

Timing conversion in this work follows (7), the one based on the center of offset, since it evenly distributes the timing error across M tunable clocks, requiring a smaller delay tuning range than (6), where the first channel is chosen as reference.

III. Stationarity-Based Blind Method

In general, looking at the TI-ADC output alone does not uniquely determine converter mismatches, since there are many input-mismatch combinations that will yield the same TI-ADC output. It is necessary, therefore, to constrain the permissible input signal to a proper subset of all Nyquist-bandlimited signals. We want these constraints to be weak enough to admit as large a class of signals as possible, yet strong enough to enable blind mismatch detection. How to constrain the input signal is an important question and one worthy of attention, since this determines the practicality and complexity of the blind algorithm. One of the previously proposed approaches is to constrain the input signal bandwidth in the frequency domain, inspired by the frequency-translation action of mismatch in (4). The unoccupied portion of the input spectrum plays the role of aliasing (thus mismatch) detector. Some recent techniques require only a small fraction of extra bandwidth, minimizing input spectrum loss. It remains unclear, however, as to the effect of out-of-band interferers (for example, signal harmonics, adjacent-channel residual power, thermal noise, and so on) in real-life signals, especially when the anti-aliasing filter is not perfect. In this paper, we take a time-domain view of TI-ADC artifacts; that is, we focus on a periodic modulation of the input by converter mismatches.

Under the assumption of WSS TI-ADC input, output autocorrelation plays the role of a mismatch indicator. Thus, the proposed technique can be best introduced by first examining the properties of TI-ADC output autocorrelation.

Since the input $x(t)$ is a WSS, its autocorrelation is shift-independent and thus depends only on the time lag between two samples. Consequently, the autocorrelation of $x(t)$ is

$$R_x(\tau) = E\left[x(t+\tau)\cdot x(t)\right] \quad \text{for all } t.$$

With nonzero residual mismatches, the TI-ADC output $z[n]$ no longer satisfies WSS properties, and its autocorrelation is shift-dependent. Specifically, we focus on the subset of TI-ADC output autocorrelations with zero and unit lag, $R_{z,k}[0]$ and $R_{z,k}[1]$, referenced to each channel as follows:

$$R_{z,k}[0] = E\left[z_k^2[n]\right], \tag{8}$$

$$R_{z,k}[1] = \begin{cases} E\left[z_k[n]z_{k+1}[n]\right] & \text{for } k = 0, \ldots, M-2, \\ E\left[z_k[n]z_0[n+1]\right] & \text{for } k = M-1. \end{cases} \tag{9}$$

These can be rewritten in terms of the input autocorrelation, $R_x(\tau)$, by using (2), as follows:

$$R_{z,k}[0] = \left(\frac{G_k^*}{\tilde{G}_k}\right)^2 R_x(0), \tag{10}$$

$$R_{z,k}[1] = \frac{G_k^* G_{(k+1) \bmod M}^*}{\tilde{G}_k \tilde{G}_{(k+1) \bmod M}} \left(R_x(T_s) + \left(\delta_k^* - \tilde{\delta}_k\right) \left.\frac{dR_x}{d\tau}\right|_{\tau=T_s} \right). \tag{11}$$

The first-order approximation in (11) is valid if δ_k^* and $\tilde{\delta}_k$ are much smaller than T_s. Note that $R_{z,k}[0]$ is a function of only gain mismatch, but $R_{z,k}[1]$ depends on both gain and timing errors. The following important observations are made from (10)–(11):

1) *No residual mismatch condition*. If there are no residual mismatches, then $R_{z,0}[m] = R_{z,1}[m] \ldots = R_{z,M-1}[m]$ for $m = 0$. In other words, the $R_{z,k}[m]$'s are equalized across channels, and shift-independence has been attained.
2) *Equalized autocorrelation condition*. If all the $R_{z,k}[m]$'s are equalized (m = 0, 1), then gain and timing estimates are equal to their intrinsic namesakes up to a common scale factor and time delay, respectively; that is, $\tilde{G}_0/G_0^* = \tilde{G}_1/G_1^* = \ldots \tilde{G}_{M-1}/G_{M-1}^*$, and $\Delta\tilde{t}_0 - \Delta t_0^* = \Delta\tilde{t}_1 - \Delta t_1^* = \ldots \Delta\tilde{t}_{M-1} - \Delta t_{M-1}^*$.
3) Therefore, if we disregard common time delay and scaling, 1) and 2) establish the following: the attainment of equalization of $R_{z,k}[0]$'s and $R_{z,k}[1]$'s is necessary and sufficient for perfect mismatch correction.

The equivalence condition in 3) is a key result that the proposed method is based on. Next, the actual adaptive algorithm used to achieve the output correlation equalization will be discussed.

IV. Adaptive Estimation Algorithm

For adaptation to time-varying mismatch errors, the algorithm will be iterative in nature. Starting from an initial estimate, the calibration loop will gradually refine parameter estimates until the zero- and unit-lag output correlation coefficients are all equalized. The equivalence result in Section III then guarantees that the estimates are equal to true parameters up to a common scale and time delay.

1. Empirical Output Autocorrelation

The calibration cycle starts with the procurement of the output autocorrelation coefficients ($R_{z,k}[0]$'s and $R_{z,k}[1]$). Given a batch of subconverter outputs, $y_k[n]$, the gain-corrected stream $z_k[n]$ is calculated from (1). The output correlation coefficients are then empirically obtained by

$$R_{z,k}^{(i)}[0] = \frac{1}{N}\sum_{n=0}^{N-1} z_k^{(i)}[n]^2, \tag{12}$$

$$R_{z,k}^{(i)}[1] = \begin{cases} \dfrac{1}{N}\displaystyle\sum_{n=0}^{N-2} z_k^{(i)}[n] z_{k+1}^{(i)}[n] & \text{for} \quad k = 0, \ldots, M-2, \\ \dfrac{1}{N}\displaystyle\sum_{n=0}^{N-2} z_k^{(i)}[n] z_0^{(i)}[n+1] & \text{for} \quad k = M-1, \end{cases} \tag{13}$$

where the superscript indicates that the calculation is based on the *i*th iteration batch data. For simpler notation, this superscript will be dropped afterwards unless necessary for clarity.

2. Equalization Reference

Given the two sets of empirical correlation coefficients from (12)–(13), we want to choose an appropriate equalization reference for each set against which empirical coefficients are compared. One of the sensible choices is the following average coefficients:

$$R_{z,ref}[0] = \frac{1}{M}\sum_{k=0}^{M-1} \tilde{G}_k^2 R_{z,k}[0], \tag{14}$$

$$R_{z,ref}[1] = \frac{1}{M}\sum_{k=0}^{M-1} R_{z,k}[1], \tag{15}$$

where $R_{z,ref}[0]$ and $R_{z,ref}[1]$ is the equalization reference for the $R_{z,k}[0]$'s and $R_{z,k}[1]$'s, respectively. The reference coefficients in (14)–(15) are basically an average across channels, except for the weighting by the gain estimate in (14). In fact, $R_{z,ref}[0]$ is equal to the average correlation observed before digital gain correction; that is, at $y_k[n]$. However, using (14) is more efficient than separately observing $y_k[n]$ and calculating its autocorrelation coefficients. After plugging (10)–(11) into (14)–(15) and neglecting the common scaling factor, $R_{z,ref}[0]$ and $R_{z,ref}[1]$ can be rewritten as a function of the TI-ADC input autocorrelation; that is,

$$R_{z,ref}[0] = R_x(0), \tag{16}$$

$$R_{z,ref}[1] = R_x(T_s) \quad \text{if no residual gain error.} \tag{17}$$

3. Parameter Recursion

By subtracting (16)–(17) from (10)–(11), we have

$$R_{z,k}[0] - R_{z,ref}[0] = R_x(0)\left(\left(\frac{G_k^*}{\tilde{G}_k}\right)^2 - 1\right), \tag{18}$$

$$R_{z,k}[1] - R_{z,ref}[1] = \left.\frac{dR_x}{d\tau}\right|_{\tau=T_s}\left(\delta_k^* - \tilde{\delta}_k\right). \tag{19}$$

Here, $R_x(0)$ is the input signal power; thus, it is strictly positive for nonzero signals. It can be shown that the derivative $dR_x/d\tau$ at $\tau = T_s$ is strictly negative for signals in the odd-ordered Nyquist zones and strictly positive in the even-ordered zones. Therefore, the sign of the left-hand side of (18) and (19) uniquely determines if the current gain or timing estimate is greater or smaller than its intrinsic namesake. This leads to the following parameter update rule:

$$\tilde{G}_k^{(i+1)} = \tilde{G}_k^{(i)} + \beta_g\left(R_{z,k}^{(i)}[0] - R_{z,ref}^{(i)}[0]\right), \tag{20}$$

$$\tilde{\delta}_k^{(i+1)} = \tilde{\delta}_k^{(i)} - \beta_t\left(R_{z,k}^{(i)}[1] - R_{z,ref}^{(i)}[1]\right), \tag{21}$$

where

$$\beta_g > 0$$

and

$$\beta_t > 0 \quad \text{if } x(t) \text{ is in odd-order Nyquist zones,}$$
$$\beta_t < 0 \quad \text{otherwise.}$$

Here, $\tilde{G}_k^{(i)}$ and $\tilde{\delta}_k^{(i)}$ are the estimate of *k*th channel gain and adjacent-channel timing error at the *i*th iteration, respectively. Once the $R_{z,k}[0]$'s and $R_{z,k}[1]$'s are all equalized, then the driving term in the parenthesis in (20) and (21) is zero; hence, convergence is achieved. The stability and speed of convergence is controlled by β_g and β_t, which will be referred to as convergence parameters. Note that the use of adjacent-channel timing parameters decouples the parameter updates for each channel.

The calculation of $2M$ correlation coefficients is practically all that is necessary for a single parameter update. This is significantly more efficient than previous blind techniques. The recursion rule in (20) and (21) also yields faster convergence than finite-difference methods or general search algorithms, because parameter adjustment is made with *a priori* known direction of decreasing residual error.

4. Convergence Analysis

Let's define $\gamma_k^{(i)}$ and $\varepsilon_k^{(i)}$ as residual gain and adjacent-channel timing error at the *i*th iteration, respectively. Then, we have

$$\gamma_k^{(i)} = \tilde{G}_k^{(i)} - G_k^*, \tag{22}$$

$$\varepsilon_k^{(i)} = \tilde{\delta}_k^{(i)} - \delta_k^*. \tag{23}$$

Then, from (18)–(21), it can be shown that $\gamma_k^{(i)}$ and $\varepsilon_k^{(i)}$ each follow a uniquely different geometric series under a small-mismatch regime.

$$\gamma_k^{(i)} = \left[1 - 2\beta_g R_x(0)\right]^i \gamma_k^{(0)}, \tag{24}$$

$$\varepsilon_k^{(i)} = \left[1 - \beta_t\left|\frac{dR_x}{d\tau}\right|_{\tau=T_s}\right]^i \varepsilon_k^{(0)}. \tag{25}$$

The effect of residual gain error is neglected in (25), for simplicity. The magnitude of the geometric ratios in (24)–(25) should be less than one so as to ensure convergence. For monotonic convergence, which is usually preferred over an oscillatory one, β_g and β_t must lie in the following range:

$$0 < \beta_g < \frac{1}{2R_x(0)}, \tag{26}$$

$$0 < \beta_t < \frac{1}{\left|\frac{dR_x}{d\tau}\right|_{\tau=T_s}}. \quad (27)$$

It is seen from the above that small values of β_g and β_t will, in general, guarantee monotonic convergence. Large values of β_g and β_t will speed up convergence as long as (26) and (27) are satisfied. This will, however, necessarily amplify noise from the driving term (the one in the parenthesis in (20) and (21)), making the parameter estimates also noisy. With β_g and β_t fixed, the gain and timing estimate will converge faster with higher input power and fast-changing input signal, respectively, since the residual errors in (24) and (25) will diminish faster.

5. Other Considerations

For simplicity, previous analysis assumed no gain mismatch when discussing the timing estimate convergence. Equation (11) suggests that nonzero residual gain error may bias timing error estimates. However, as long as the gain calibration loop is in action, the timing estimates will eventually converge to a true parameter (see Section V for experimental results).

There are several factors that will affect parameter estimation: ADC quantization noise, sampling clock random jitter, autocorrelation estimation error due to finite observation, finite-resolution sampling clock tuning, and so on. Using small values of β_g and β_t, or increasing the batch size N, in general, decreases the contribution of these noise sources. However, the sampling clock quantization error can only be reduced by increasing its resolution. The minimum tuning resolution should be commensurate with the target signal-to-noise ratio (SNR) or Spurious-Free Dynamic Range (SFDR) level. For example, 80 dB of target SNR requires $0.00003T_s$ of timing control resolution (assuming the input sinusoid is at $f_s/2$). If the delay control range is 0.03 T_s, for instance, then approximately 1,000 quantization levels (that is, 10-bit level) will be necessary. Other than the minimum resolution requirement, the proposed calibration scheme is tolerant to analog imperfections in clock tuning circuitry. For example, the precise tuning curve need not be known. It can even change between calibration cycles since the feedback action of the blind calibration will eventually track such variations.

V. Experimental Results

Figure 3 shows the $M = 4$ TI-ADC experimental setup. Four 14-bit 100 MSPS commercial ADC's (AD6645 from Analog Devices, Inc.) are used to achieve 400 MSPS of overall sampling rate. The logic analyzer performs both data acquisition and digital signal processing. The four-phase sampling clock is derived from a single 100 MHz reference clock, followed by a voltage-controlled delay line. Each tunable line consists of a single 50 Ω T-section (L-C-L) with varactor diodes (MV104 from ON Semiconductor) for delay control. The delay line provides $0.2T_s$ ($T_s = 2.5$ ns) of delay tuning range across 0 V to 3 V of tuning voltage.

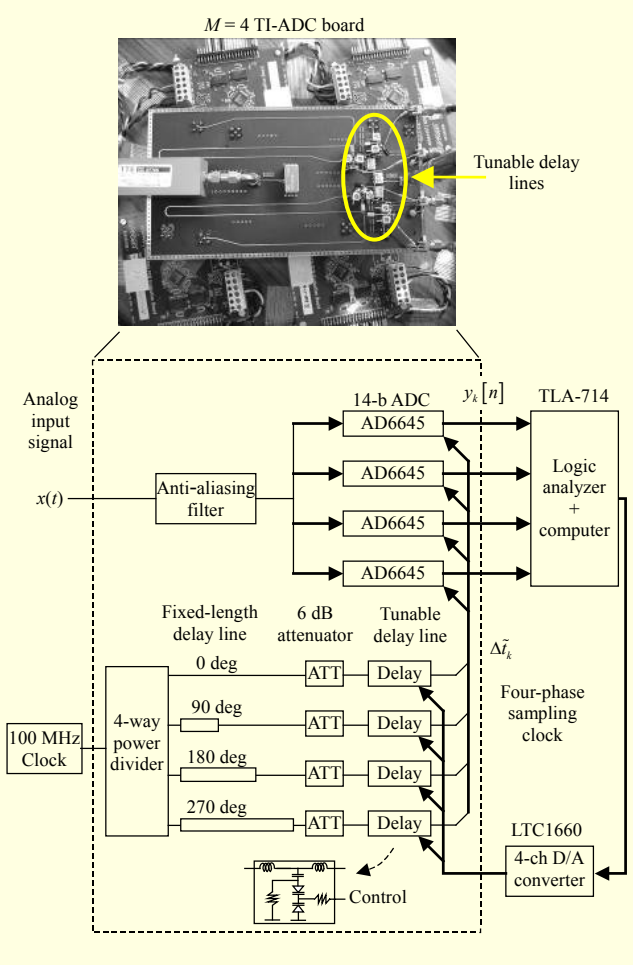

Fig. 3. Experimental setup for $M = 4$ 400-MSPS TI-ADC with proposed blind adaptive calibration loop. Sampling clock is fine-tuned by a single L-C-L section of varactor-loaded delay line. 6 dB attenuators minimize impedance variation with varactor tuning, thus preventing undesirable cross-line tuning effects.

1. Narrowband Input Test

Sinusoids are used as a representative narrowband input signal. Convergence parameters are chosen to be one tenth of the stability limit given by (26)–(27) (β_g, $\beta_t \approx 0.2$). The batch size for all narrowband tests is $N = 4{,}096$.

First, a 171.567 MHz sinusoid is applied at the TI-ADC input, and the blind calibration loop is initiated. Figure 4 shows

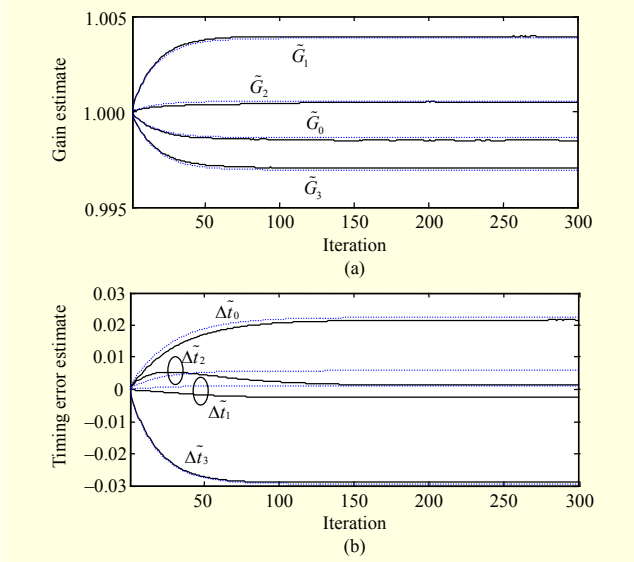

Fig. 4. Measured convergence plot of (a) gain and (b) timing error estimates with a 171.567 MHz sinusoidal input. Solid lines represent measurement. Dotted lines denote predicted curves by (22)–(25) with intrinsic gain [0.99865, 1.0038, 1.0005, 0.99695], and sampling timing errors [$0.0224T_s$, $0.0012T_s$, $0.0058T_s$, $-0.0294T_s$] characterized at 172.8 MHz by a training method [6].

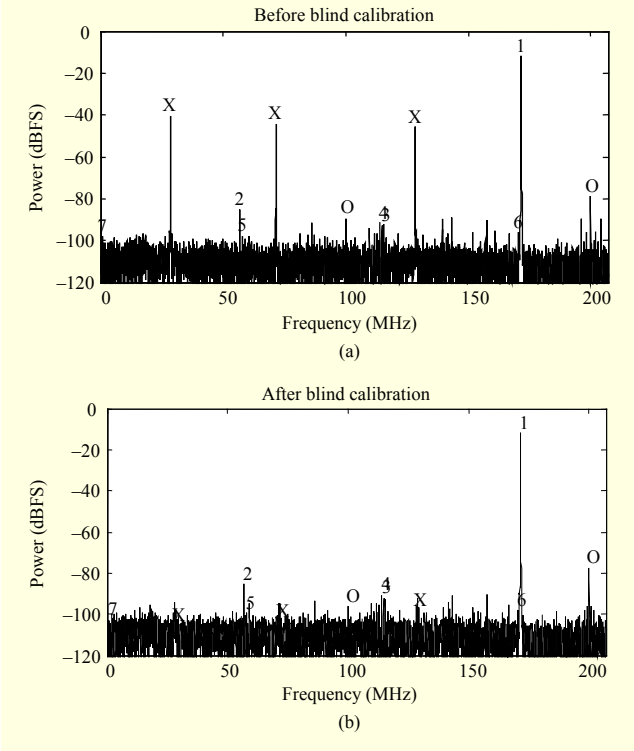

Fig. 5. Measured TI-ADC output spectrum with a 171.567 MHz input (marked with '1'): (a) before and (b) after 300 iterations (N = 4,096). Gain and sampling time mismatch spurs are labeled with 'X.' The offset spurs are represented by 'O,' and the input signal harmonics up to the 7th order are also shown as numbers.

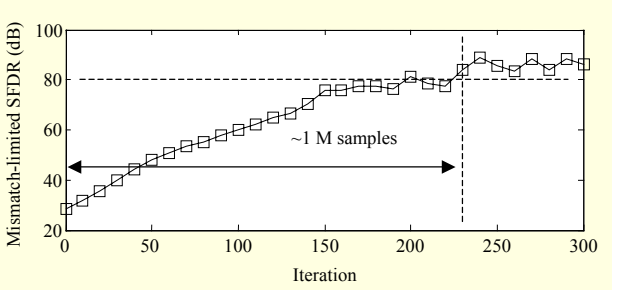

Fig. 6. Improvement of mismatch-limited SFDR during 300 iterations with a 171.567 MHz sinusoid input (N = 4,096).

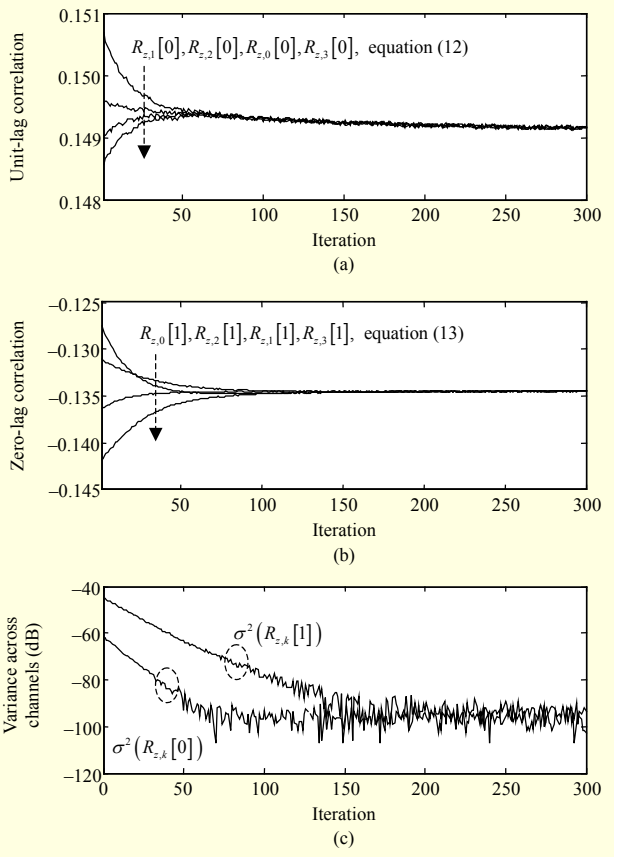

Fig. 7. Measured equalization plot of (a) unit-lag, (b) zero-lag correlation coefficients, and (c) their cross-channel variance. Input signal is a sinusoid at 171.567 MHz.

the measured convergence curve for gain and sampling time error estimate. It is seen that the measurement (solid lines) closely follows the prediction (dotted lines). The small discrepancy in timing convergence plot is due to the slight curvature in the delay tuning characteristic (the prediction assumes linear tuning). Figure 5 shows the TI-ADC output spectrum before and after 300 calibration iterations. We define the following performance-evaluation metric, disregarding mismatch-irrelevant spurs:

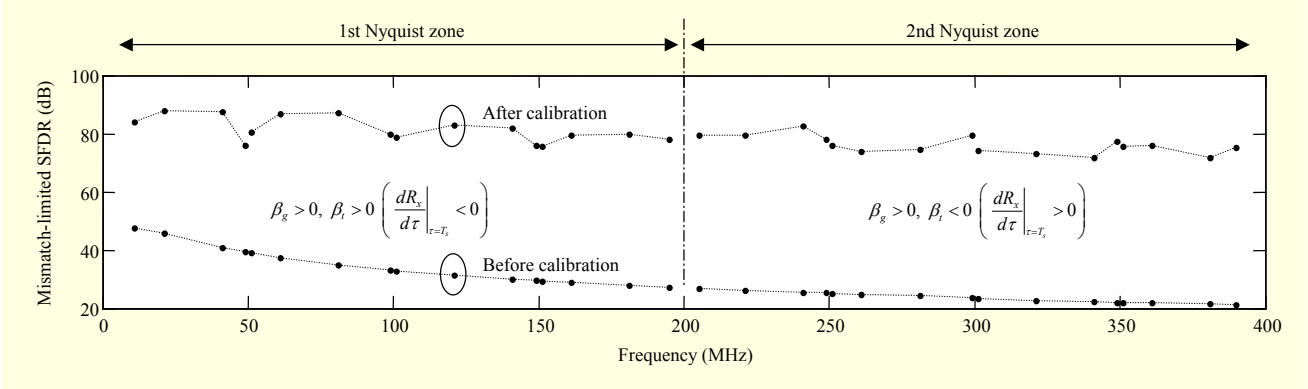

Fig. 8. Single-tone test result across the first two Nyquist zones (N = 4,096). The sign of the correlation derivative and convergence parameters is also shown (see (26), (27)). The input anti-aliasing filter in Fig. 3 (cutoff = 187 MHz) was removed for this test.

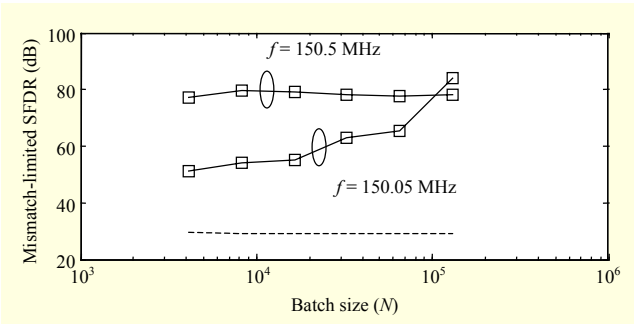

Fig. 9. Single-tone calibration performance near 150 MHz input, which is one of the failure frequencies (50 MHz, 100 MHz, and 150 MHz). The closer the input frequency approaches to 150 MHz, the greater the required batch size. Dotted line is uncalibrated performance.

$$\text{Mismatch-limited SFDR} = \frac{\text{signal power}}{\max(\text{mismatch spur power})}.$$

Thus, mismatch-limited SFDR (ML-SFDR) is the maximum achievable SFDR in the absence of other spurious tones. The proposed calibration suppressed mismatch spurs by more than 40 dB, achieving a value of more than 80 dB of ML-SFDR (Fig. 6). Note that the initial linear increase (in dB scale) comes from exponential parameter convergence. The equalization process of the output correlation coefficients is shown in Fig. 7.

Next, the frequency of the input sinusoid is swept across the first two Nyquist zones (10 MHz to 390 MHz), with the same batch size of N = 4,096 (Fig. 8). Up to 70 dB to 90 dB of SFDR is obtained.

There are three frequencies in the first Nyquist zone where the stationary input assumption fails for M = 4: 50 MHz, 100 MHz, and 150 MHz. As the input sinusoid comes closer to one of these frequencies, a longer batch size is required to maintain calibration performance. Calibration performance versus batch size near to 150 MHz is investigated in Fig. 9. No performance loss is observed down to 150.5 MHz. If the input

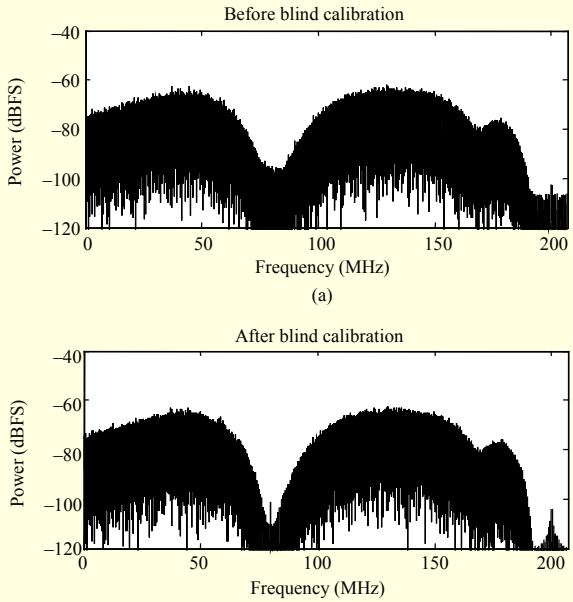

Fig. 10. Measured TI-ADC output spectrum with a dc to 180 MHz wideband input signal: (a) before and (b) after 1,200 iterations (N = 131,072). The original deep notch at 80 MHz is masked by aliasing products in (a), but restored after calibration in (b), implying that the mismatch is corrected.

is at 150.05 MHz, however, then the ML-SFDR drops down to 50 dB (still 20 dB of calibration gain, though), and at least $N = 10^5$ is necessary to regain 80 dB of the ML-SFDR level. In summary, the batch size N = 4,096 can meet 80 dB of single-tone ML-SFDR requirement over 98.5% of the entire Nyquist band. If a longer observation of up to $N = 10^5$ is allowed, then the spectral performance is maintained over 99.85% of the bandwidth.

2. Wideband Input Test

An independent, identically distributed sequence is first

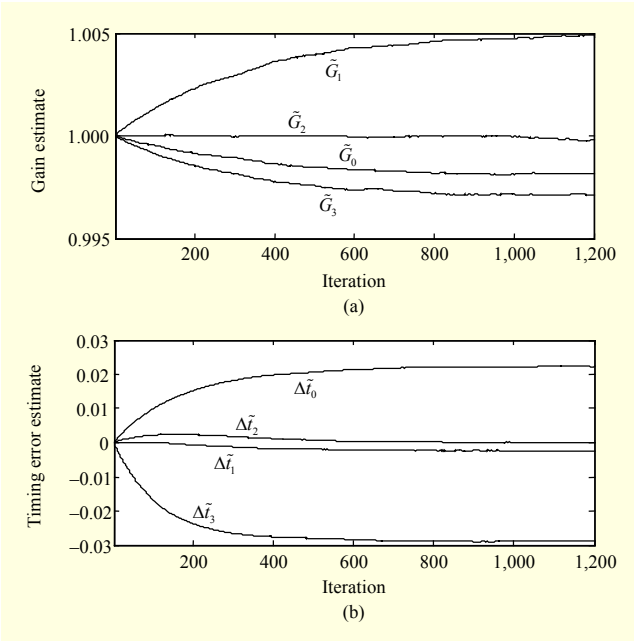

Fig. 11. Measured convergence plot of (a) gain and (b) timing error estimates with the wideband input signal in Fig. 10 (N = 131,072).

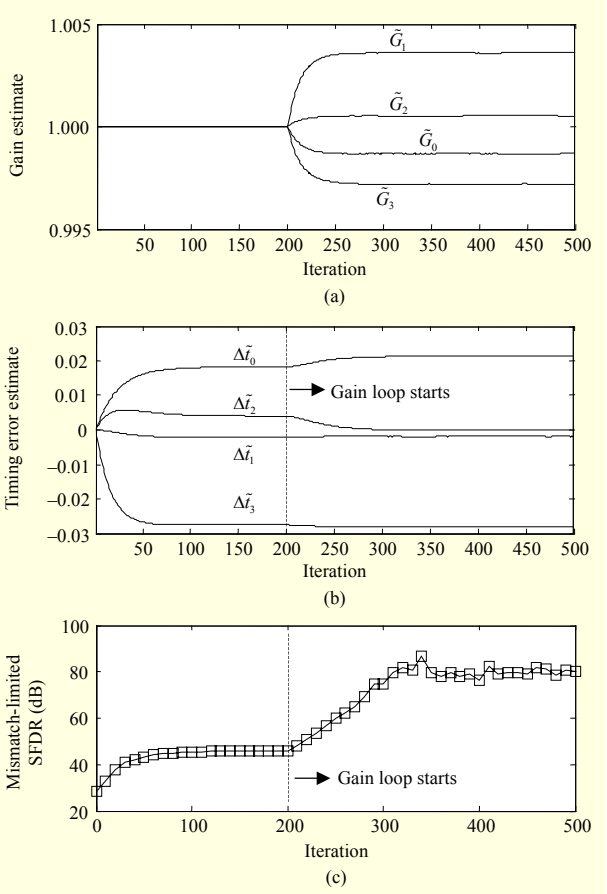

Fig. 12. Measured convergence plot with a 171.567 MHz sine input: (a) gain and (b) timing error estimate. Gain adaptation is intentionally delayed by 200 iterations to see its effect on timing error convergence.

generated by an arbitrary waveform generator and then filtered by a 10-tap finite impulse response (FIR) filter. Its occupied bandwidth is approximately 180 MHz. Unlike sinusoidal inputs, wideband input signals mostly overlap with their own aliasing products. For the purpose of alias identification, a deep notch is created at 80 MHz. Before calibration, there exist significant channel mismatches, and the notch at 80 MHz is partially filled with frequency-shifted input spectra, as given by (4) (Fig. 10(a)). After 1,200 iterations, the calibration suppresses any aliasing products, and the deep notch is restored, as seen in Fig. 10(b). Parameter convergence plots are shown in Fig. 11. Note that the batch size N = 131,072 is much longer than the narrowband case. This is because empirical correlation coefficients for wideband signals are noisier than narrowband ones, in general.

3. Effects of Residual Gain Error on Timing Curve

As a final test, the timing calibration loop is first initiated with a 171.567 MHz sine input, with gain correction turned off (Fig. 12). In Fig. 12(b), timing estimates are seen to converge with bias in the presence of residual gain error. After 200 iterations, a gain correction loop begins (Fig. 12(a)), when timing parameters also start readjusting themselves. After another 100 iterations, both gain and timing estimates achieved convergence to a true parameter. Under a small-mismatch regime, in general, residual gain error does not significantly affect the convergence of timing parameters, as experimentally verified by Figs. 12(b) and (c).

VI. Conclusion

We have demonstrated a new adaptive blind technique for multi-channel TI-ADCs. The analog-domain correction of timing mismatches, combined with autocorrelation-based error detection, dramatically reduces hardware and computational complexity. Specifically, empirical calculation of $2M$ output autocorrelation coefficients is practically enough for a single parameter update. After blind mismatch correction, 70 dB to 90 dB of SFDR was experimentally achieved across the first two Nyquist zones. Proof of parameter convergence is given under the WSS input assumption. There is no restriction in the number of TI-ADC channels or input signal bandwidth.

References

[1] W.C. Black and D.A. Hodges, "Time Interleaved Converter

Arrays," *IEEE J. Solid-State Circuits*, vol. 15, no. 6, Dec. 1980, pp. 1022–1029.

[2] K. Poulton et al., "A 20 GS/s 8 b ADC with a 1 MB Memory in 0.18 μm CMOS," *IEEE Int. Solid-State Circuits Conf.*, San Francisco, CA, USA, Feb. 13, 2003, pp. 318–496.

[3] A. Petraglia and S.K. Mitra, "Analysis of Mismatch Effects among A/D Converters in a Time-Interleaved Waveform Digitizer," *IEEE Trans. Instrum. Meas.*, vol. 40, no. 5, Oct. 1991, pp. 831–835.

[4] N. Kurosawa et al., "Explicit Analysis of Channel Mismatch Effects in Time-Interleaved ADC Systems," *IEEE Trans. Circuits Syst. I, Fundam. Theory Appl.*, vol. 48, no. 3, Mar. 2001, pp. 261–271.

[5] C. Vogel and H. Johansson, "Time-Interleaved Analog-to-Digital Converters: Status and Future Directions," *IEEE Int. Symp. Circuits Syst.*, Kos Island, Greece, May 21–24, 2006, pp. 3386–3389.

[6] M. Seo, M. Rodwell, and U. Madhow, "Comprehensive Digital Correction of Mismatch Errors for a 400-Msamples/s, 80-db SFDR Time-Interleaved Analog-to-Digital Converter," *IEEE Trans. Microw. Theory Techn.*, vol. 53, no. 3, Mar. 2005, pp. 1072–1082.

[7] S.M. Jamal et al., "A 10-b 120-Msample/s Time-Interleaved Analog-to-Digital Converter with Digital Background Calibration," *IEEE J. Solid-State Circuits*, vol. 37, no. 12, Dec. 2002, pp. 1618–1627.

[8] S.M. Jamal et al., "Calibration of Sample-Time Error in a Two-Channel Time-Interleaved Analog-to-Digital Converter," *IEEE Trans. Circuits Syst. I, Reg. Papers*, vol. 51, no. 1, Jan. 2004, pp. 130–139.

[9] J. Matsuno et al., "All-Digital Background Calibration Technique for Time-Interleaved ADC Using Pseudo Aliasing Signal," *IEEE Trans. Circuits Syst. I, Reg. Papers*, vol. 60, no. 5, May 2013, pp. 1113–1121.

[10] V. Divi and G. Wornell, "Blind Calibration of Timing Skew in Time-Interleaved Analog-to-Digital Converters," *IEEE J. Sel. Topics Signal Process.*, vol. 3, no. 3, June 2009, pp. 509–522.

[11] J. Elbornsson, F. Gustafsson, and J.-E. Eklund, "Blind Adaptive Equalization of Mismatch Errors in a Time-Interleaved A/D Converter System," *IEEE Trans. Circuits Syst. I, Reg. Papers*, vol. 51, no. 1, Jan. 2004, pp. 151–158.

[12] S. Saleem and C. Vogel, "Adaptive Blind Background Calibration of Polynomial-Represented Frequency Response Mismatches in a Two-Channel Time-Interleaved ADC," *IEEE Trans. Circuits Syst. I, Reg. Papers*, vol. 58, no. 6, June 2011, pp. 1300–1310.

[13] C. Law, P. Hurst, and S. Lewis, "A Four-Channel Time-Interleaved ADC with Digital Calibration of Interchannel Timing and Memory Errors," *IEEE J. Solid-State Circuits*, vol. 45, no. 10, Oct. 2010, pp. 2091–2103.

[14] S. Huang and B.C. Levy, "Adaptive Blind Calibration of Timing Offset and Gain Mismatch for Two-Channel Time-Interleaved ADCs Converters," *IEEE Trans. Circuits Syst. I, Reg. Papers*, vol. 53, no. 6, June 2006, pp. 1278–1288.

[15] S. Huang and B.C. Levy, "Blind Calibration of Timing Offsets for Four-Channel Time-Interleaved ADCs," *IEEE Trans. Circuits Syst. I, Reg. Papers*, vol. 54, no. 4, Apr. 2007, pp. 863–876.

[16] M. Seo, M. Rodwell, and U. Madhow, "Blind Correction of Gain and Timing Mismatches for a Two-Channel Time-Interleaved Analog-to-Digital Converter," *Asilomar Conf. Signals, Syst. Comput.*, Pacific Grove, CA, USA, Oct. 2005, pp. 1121–1125.

[17] M. Seo, M. Rodwell, and U. Madhow, "Blind Correction of Gain and Timing Mismatches for a Two-Channel Time-Interleaved Analog-to-Digital Converter: Experimental Verification," *IEEE Int. Symp. Circuits Syst.*, Kos Island, Greece, May 21–24, 2006, pp. 3394–3397.

[18] D. Fu et al., "A Digital Background Calibration Technique for Time-Interleaved Analog-to-Digital Converters," *IEEE J. Solid-State Circuits*, vol. 33, no. 12, Dec. 1998, pp. 1904–1911.

[19] K.C. Dyer et al., "An Analog Background Calibration Technique for Time-Interleaved Analog-to-Digital Converters," *IEEE J. Solid-State Circuits*, vol. 33, no. 12, Dec. 1998, pp. 1912–1919.

[20] H. Jin and E.K.F. Lee, "A Digital-Background Calibration Technique for Minimizing Timing-Error Effects in Time-Interleaved ADCs," *IEEE Trans. Circuits Syst. II, Analog Digit. Signal Process.*, vol. 47, no. 7, July 2000, pp. 603–613.

[21] E. Iroaga, B. Murmann, and L. Nathawad, "A Background Correction Technique for Timing Errors in Time-Interleaved Analog-to-Digital Converters," *IEEE Int. Symp. Circuits Syst.*, Kobe, Japan, vol. 6, May 23–26, 2005, pp. 5557–5560.

[22] C.-C. Huang, C.-Y. Wang, and J.-T. Wu, "A CMOS 6-Bit 16-GS/s Time-Interleaved ADC Using Digital Background Calibration Techniques," *IEEE J. Solid-State Circuits*, vol. 46, no. 4, Apr. 2011, pp. 848–858.

[23] D. Camarero et al., "Mixed-Signal Clock-Skew Calibration Technique for Time-Interleaved ADCs," *IEEE Trans. Circuits Syst. I, Reg. Papers*, vol. 55, no. 11, Dec. 2008, pp. 3676–3687.

[24] A. Haftbaradaran and K. Martin, "A Background Sample-Time Error Calibration Technique Using Random Data for Wide-Band High-Resolution Time-Interleaved ADCs," *IEEE Trans. Circuits Syst. II, Exp. Briefs*, vol. 55, no. 3, Mar. 2008, pp. 234–238.

[25] M. El-Chammas and B. Murmann, "A 12-GS/s 81-mW 5-Bit Time-Interleaved Flash ADC with Background Timing Skew Calibration," *IEEE J. Solid-State Circuits*, vol. 46, no. 4, Apr. 2011, pp. 838–847.

[26] M. Seo, M. Rodwell, and U. Madhow, "A Low Computation Adaptive Blind Correction for Time-Interleaved ADCs," *IEEE Int. Midwest Symp. Circuits Syst.*, San Juan, Puerto Rico, Aug. 6–9, 2006, pp. 292–296.

Munkyo Seo received his BS and MS degrees in electronics engineering from Seoul National University, Rep. of Korea, in 1994 and 1996, respectively. He received his PhD degree in electrical engineering from the University of California, Santa Barbara (UCSB), CA, USA, in 2007. From 1997 to 2002, he was an RF engineer with LG Electronics Inc., Anyang, Rep. of Korea, designing microwave subsystems for wireless communication. He was an assistant project scientist with UCSB from 2008 to 2009. In 2009, he joined Teledyne Scientific Company, Thousand Oaks, CA, USA, where he worked on the design of various millimeter-wave, terahertz, and high-speed mixed-signal circuits. Since 2013, he has been with Sungkyunkwan University, Suwon, Rep. of Korea, as an assistant professor.

Eunsoo Nam received his BS degree in physics from Kyungpook National University, Daegu, Rep. of Korea, in 1983 and his MS and PhD degrees in physics from the State University of New York, Buffalo, NY, USA, in 1992 and 1994, respectively. In 1994, he joined the Electronics and Telecommunications Research Institute (ETRI), Daejeon, Rep. of Korea, where his research involved compound semiconductor devices, including GaAs-and GaN-based high-frequency power device platforms, long wavelength InP semiconductor photonic devices, optoelectronic integrated circuits for microwave circuits, and SDN network devices. In 2006, he was a visiting scholar at the Division of Engineering and Applied Sciences, Harvard University, Cambridge, MA, USA. His current research interest is to combine radio and optics technologies to develop millimeter-wave photonic components and integrated functions for a number of applications, including broadband communications, radar, security, and instrumentation. He is now a senior vice president managing the materials and devices R&D department at ETRI.

Mark Rodwell received his PhD degree from Stanford University, CA, USA, in 1988. He holds the Doluca Family Endowed Chair in Electrical and Computer Engineering at the University of California, Santa Barbara (UCSB), CA, USA. He directs the UCSB node of the NSF Nanofabrication Infrastructure Network, and the SRC Nonclassical CMOS Research Center. His research group works to extend the operation of integrated circuits to the highest feasible frequencies. He received the 2010 IEEE Sarnoff Award for the development of InP-based bipolar IC technology for mm-wave and sub-mm-wave applications. His group's work on GaAs Schottky-diode ICs for subpicosecond/mm-wave instrumentation was awarded the 1997 IEEE Microwave Prize.